청정환경기술

Synthesis of Titanate Nanotubes Via A Hydrothermal Method and Their Photocatalytic Activities

Ye Eun Kim[1,2], Mi Yeon Byun[3], Kwan-Young Lee[2], and Man Sig Lee[1,4,*]

[1]Ulsan Division, Korea Institute of Industrial Technology (KITECH)
Ulsan 44413, Republic of Korea
[2]Department of Chemical and Biological Engineering, Korea University
Seoul 02841, Republic of Korea
[3]Center of Environmentally Beneficial Catalysis, The University of Kansas
Lawrence, KS, 66047, USA
[4]Department of Green Process and System Engineering, University of Science and Technology (UST)
Ulsan 44413, Republic of Korea

Abstract

Titanate nanotubes (TNTs) were synthesized via alkaline hydrothermal treatment using commercial TiO_2 nanoparticles (P25). The TNTs were prepared at various TiO_2/NaOH ratios, hydrothermal temperatures, and hydrothermal times. The synthesized catalysts were characterized by X-ray diffraction, field-emission scanning electron microscopy, N_2 adsorption-desorption isotherms, field-emission transmission electron microscopy, and ultraviolet-visible spectroscopy. TNTs were generated upon a decrease in the TiO_2/NaOH ratio due to the dissolution of TiO_2 in the alkaline solution and the generation of new Ti-O-Ti bonds to form titanate nanoplates and nanotubes. The hydrothermal treatment temperature and time were important factors for promoting the nucleation and growth of TNTs. The TNT catalyst with the largest surface area ($389.32 \text{ m}^2 \text{ g}^{-1}$) was obtained with a TiO_2/NaOH ratio of 0.25, a hydrothermal treatment temperature of 130 ℃, and a hydrothermal treatment time of 36 h. Additionally, we investigated the photocatalytic activity of methyl violet 2B (MV) over the TNT catalysts under UV irradiation and found that the degradation efficiencies of the TNTs were higher than that of P25. Among the TNT catalysts, the TNT catalyst that was hydrothermally synthesized for 36 h (TNT 36 h) exhibited a 96.9% degradation efficiency and a degradation rate constant that was 4.8 times higher than P25 due to its large surface area, which allowed for more contact between the MV molecules and TNT surfaces and facilitated rapid electron transfer. Finally, these results were correlated with the specific surface area.

Keywords : Hydrothermal, Methyl violet, Photocatalyst, Titanate nanotube

1. Introduction

TiO$_2$ has been widely used in photocatalysis, supercapacitors, and lithium-ion batteries owing to its photosensitivity, non-toxicity, and chemical stability [1-3]. In recent decades, many researchers have attempted to synthesize zero-dimensional TiO_2 nanoparticles owing to their large surface areas. Recently, higher-dimensional TiO_2 materials such as fibers, tubes, and rods, which are expected to exhibit higher catalytic activity due to their large surface areas, pore sizes, and pore volumes, have been reported as promising materials for various applications. Among the various structures, one-dimensional (1D) titanate nanotubes (TNTs) have a nanostructure similar to that of carbon nanotubes, with novel electronic and physical properties. 1D TiO_2 nanostructures have a relatively small amount of grain boundaries, which can act as single crystal and reduce the grain boundary effect. The low surface intact in 1D structures can lead to a large interface charge-transfer resistance compared to nanoparticles [4,5]. Li et al. prepared TiO_2 nanorod by a hydrothermal method and performed photodegradation over TiO_2 nanoparticle and nanorod, respectively. The photocatalytic activity of nanoparticle was lower than that of nanorod owing to a tendency to agglomerate and reduce the surface area, facilitating the recombination of photoinduced charges [6]. Yu and co-workers reported that TiO_2 nanotube had the prolonged lifetime of

photoinduced electrons and efficient separation of photoinduced charge carriers due to the large surface area [7]. Thus, the photocatalytic activity can be affected by the dimensional effect.

The formation of TNT was first reported by Kasuga et al. using alkali hydrothermal methods in 1998 [8]. Since then, various methods have been used to produce TNTs including the hydrothermal treatment, sol-gel method, electrochemical anodic oxidation, and template-assisted method [9-12]. Among them, the hydrothermal method remains one of the simplest procedures that can produce a high yield of TNT. The unique characteristics of their 1D structures have been previously reported. Among the various morphologies, TiO_2 nanotubes have high chemical stability and photocatalytic performance and can be utilized in catalysts, photovoltaic cells, and semiconductor devices. Although several researchers have insisted that TNT formation is strongly influenced by annealing temperature, alkaline concentration, and pressure [12-15], the formation mechanism of TNTs is still debatable.

Herein, we studied the influence of the TiO_2/NaOH ratio, hydrothermal treatment temperature, and hydrothermal treatment time on the formation of TNTs and proposed the formation mechanism of TNTs based on X-ray diffraction (XRD) and field-emission scanning electron microscopy (FE-SEM) results. TNTs were successfully synthesized via an alkaline hydrothermal method using commercial TiO_2 nanoparticles (P25) as the starting material. In addition, we investigated the photocatalytic degradation of methyl violet 2B (MV) under UV irradiation to compare the photocatalytic activities of the catalysts. Finally, the specific surface area of the TNTs was correlated with the photodegradation efficiency and rate.

2. Material and methods

2.1. Materials

Commercial TiO_2 (P25) was obtained from Evonik Degussa and used as a starting material. Sodium hydroxide and hydrochloric acid were purchased from Sigma Aldrich.

2.2. Preparation of TiO_2 nanotube

TiO_2 nanotubes were prepared via a hydrothermal method using a procedure similar to that described by Kasuga et al. [8]. A certain amount of commercial TiO_2 P25 was suspended in 100 mL of 10 M NaOH and stirred for 1 h. Then, the mixture was transferred into a 200-mL Teflon-lined autoclave and hydrothermally treated at 90-150 ℃ for 24-72 h. Then, the autoclave was naturally cooled to ambient temperature. Next, the powder was collected by filtration and the residue was added to 600 mL of 0.1 M HCl and stirred for 3 h to remove sodium ions. The mixture was subsequently filtered and washed with distilled water to a pH of 7. Finally, the synthesized TiO_2 nanotubes were dried at 80 ℃ for 12 h.

Each sample was prepared by varying the experimental parameters such as TiO_2/NaOH ratio, hydrothermal temperature, and hydrothermal time.

2.3. Characterization of TiO_2 nanotube

An X-ray diffractometer (Rigaku, D/MAX 2500-V) was used to analyze the crystalline structure of the catalysts using a Cu Kα radiation source. Morphological investigations were conducted using a field-emission scanning electron microscope (JEOL, JSM-6500) and TEM (Hitachi Hightech, HT-7800) at accelerating voltages of 10 and 120 kV, respectively. The textural properties were analyzed by N_2 physisorption isotherms at 77 K using a Micromeritics ASAP 2020 instrument. Before analysis, all the samples were pretreated at 150 ℃ for 4 h under vacuum. Finally, ultraviolet-visible (UV-Vis) absorption spectra were recorded using a UV-Vis spectrophotometer (Shimadzu, UV-2550).

2.4. Photocatalytic activity

Photocatalytic performance of the catalysts was measured via the photocatalytic degradation of MV under UV light irradiation. The light source was a 20 W UV lamp with a light intensity of 1100 µW cm^{-2}. First, the catalysts were added to 50 mL of 30 ppm MV and stirred for 30 min in the dark. Upon reaching the adsorption-desorption equilibrium, the UV lamp was turned on and the samples were irradiated for 180 min. The photodegradation over pristine TiO_2 (P25) was also investigated to compare the degradation efficiency. The samples (3 mL) were filtered using a syringe filter every 30 min and the MV concentration was monitored using a UV-Vis spectrophotometer (Shimadzu, UV-2550).

3. Results and Discussion
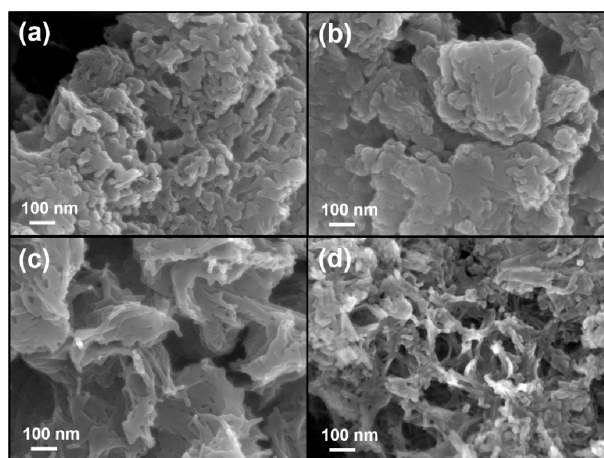
3.1. Characterization of TiO_2 nanotubes

Figure 1 shows the XRD patterns of the starting material (commercial TiO_2, P25) and the hydrothermally treated TNTs prepared at 130 ℃ for 24 h at different TiO_2/NaOH ratios. Sharp XRD peaks, as shown in Figure 1(a), were observed for the pristine P25 sample, indicating the presence of anatase (JCPDS 21-1272) and rutile (JCPDS 21-1276) phases without any impurities present. As the TiO_2/NaOH ratio decreased, the rutile and anatase peaks disappeared, and an amorphous phase was observed at $2\theta = 25$-40° [16]. At a TiO_2/NaOH ratio of 0.25, low and broad peaks at $2\theta = 24.2°$, 28.6°, and 48.3° were observed, which were indexed to the titanate form (JCPDS 44-0131) [17]. The XRD profile of the TNT sample with a TiO_2/NaOH ratio of 0.25 exhibited broader anatase and TNT peaks compared to pristine P25. The crystallinity of TNT at a TiO_2/NaOH ratio of 0.5 was significantly improved compared to those of TNTs with TiO_2/NaOH ratios of 1.0, indicating the formation of titanate forms. Based on these results, we concluded
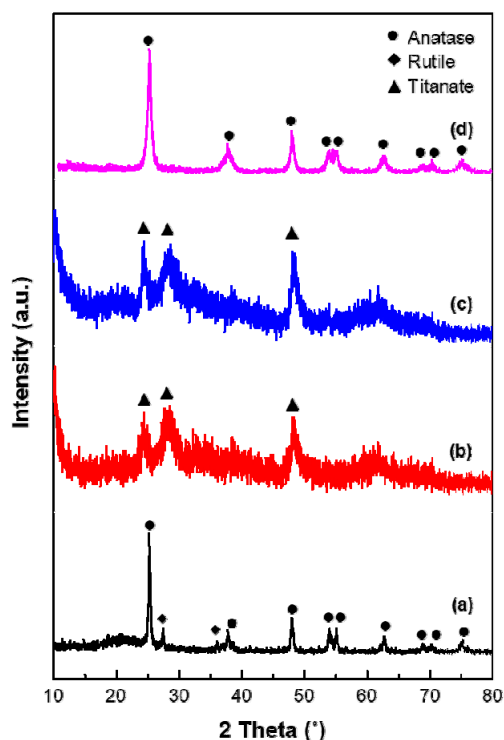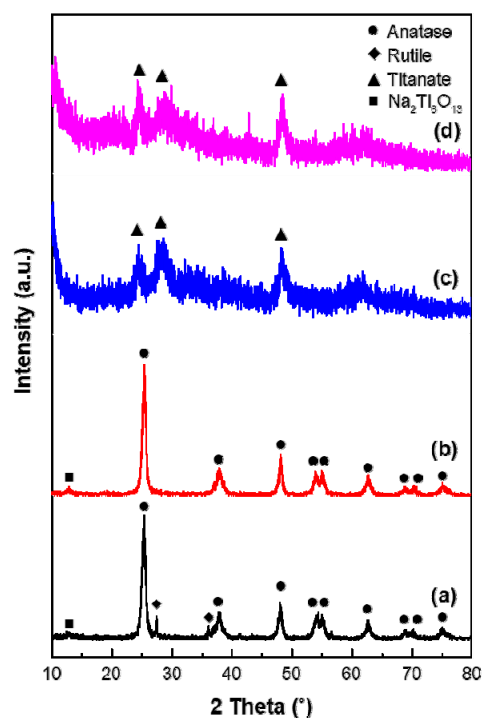
Figure 1. XRD patterns of (a) starting material (P25), and TNTs synthesized for 24 h and hydrothermal treated at 130 ℃ with different TiO₂/NaOH ratio: (b) 0.25, (c) 0.5, and (d) 1.

Figure 3. XRD patterns of TNTs synthesized for 24 h with TiO₂/NaOH ratio 0.25 at different hydrothermal treatment temperature: (a) 90 ℃, (b) 110 ℃, (c) 130 ℃, and (d) 150 ℃.

that a lower TiO_2 content was important for the transformation of polymorphs to titanate forms.

Figure 2 shows the FE-SEM images of the as-prepared samples, which were prepared at 130 ℃ for 24 h, at different TiO_2/NaOH ratios. After the alkaline hydrothermal treatment, the samples clearly exhibited a change in their morphology due to hydrothermal sintering with neighboring nanoparticles. When the TiO_2/NaOH ratio was reduced from 1.0 to 0.5, intermediate nanosheet-like


Figure 2. FE-SEM images of (a) pristine P25 in the absence of NaOH solution and TNTs synthesized for 24 h and hydrothermal treated at 130 ℃ with different TiO_2/NaOH ratio: (b) 0.25, (c) 0.5, and (d) 1.

structures were observed. This is ascribed to the dissolution of TiO_2 nanoparticles, which is achieved by breaking the original Ti-O-Ti bonds and reforming their morphology by generating new Ti-O-Ti bonds. The formation of nanotube-shaped structures was observed when the TiO_2/NaOH ratio was further reduced to 0.25. The width and length of the TNT were 7.4-10.1 nm and 100-130 nm, respectively.

The XRD profiles of TiO_2 treated at different hydrothermal temperatures are shown in Figure 3. Meanwhile, the TiO_2/NaOH ratio and hydrothermal time were fixed at 0.25 and 24 h, respectively. The structural characteristics of TNT prepared at 90 ℃ resembled those of raw TiO_2 with mixed phases of anatase and rutile. The peak at $2\theta = 13°$ was found to be $Na_2Ti_6O_{13}$ phase (JCPDS 37-0951), resulting from the reaction of TiO_2 in alkaline solution or some oligomeric species of sodium titanate via NaOH etching [18-20]. After the hydrothermal treatment at 110 ℃, the peaks corresponding to the rutile phase disappeared. Furthermore, no anatase or rutile phase was observed in the hydrothermally treated products formed at temperatures above 130 ℃. The relative intensities of the peaks were ascribed to the increase in hydrothermal temperature and were accompanied by the formation of new peaks, which are assigned to titanate forms. The peaks of the titanate forms were similar to those of alkali or hydrogen titanates, which have a monoclinic lattice. Based on these results, the optimal hydrothermal temperature was determined to be 130 ℃.
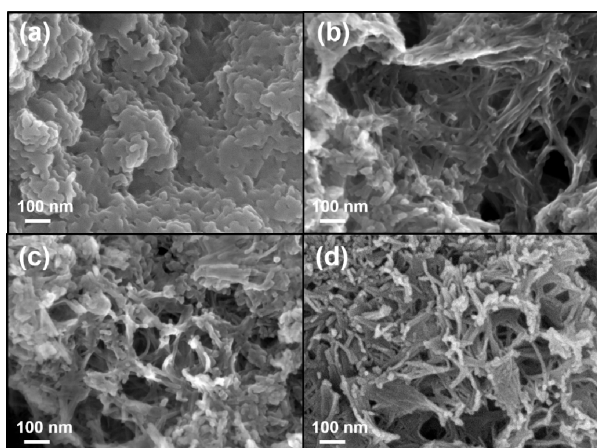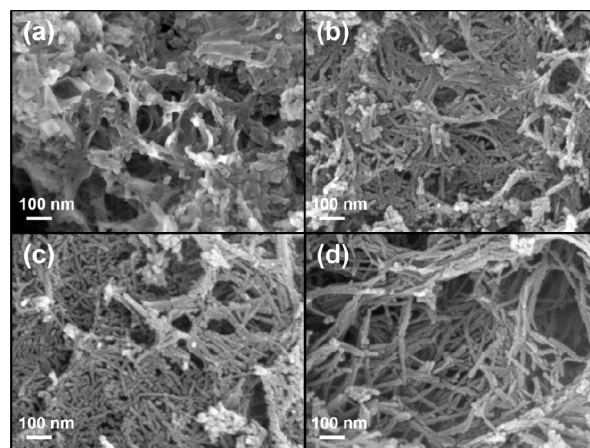
Figure 4. FE-SEM images of TNTs synthesized for 24 h with TiO$_2$/NaOH ratio 0.25 at different hydrothermal treatment temperature: (a) 90 ℃, (b) 110 ℃, (c) 130 ℃, and (d) 150 ℃.

Figure 4 shows the FE-SEM micrographs of TiO$_2$ after hydrothermal treatment at various temperatures for 24 h. No tubular structures were observed for the TNT sample prepared at 90 ℃. The length of the nanoparticles increased with increasing hydrothermal temperatures. After the hydrothermal treatment above 130 ℃, plate-like and whisker-like structures were formed and coexisted. We hypothesized that the TiO$_2$ nanoparticles gradually dissolved in a concentrated NaOH aqueous solution, with an excess amount of Na$^+$ ions, and transformed into nanosheet-like structures
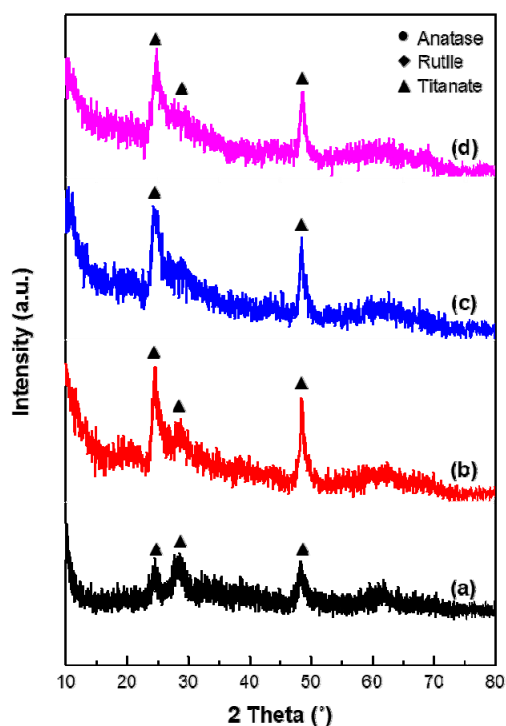
Figure 5. XRD patterns of TNTs synthesized with TiO$_2$/NaOH ratio 0.25 at 130 ℃ for different hydrothermal treatment time: (a) 24 h, (b) 36 h, (c) 60 h, and (d) 72 h.
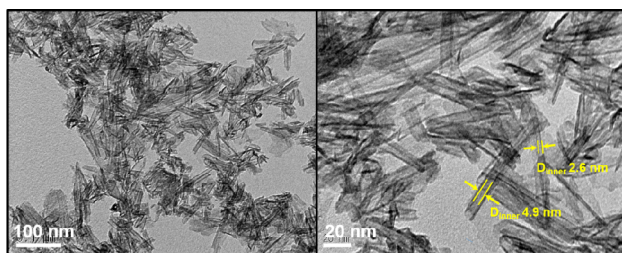

Figure 6. FE-SEM images of TNTs synthesized with TiO$_2$/NaOH ratio 0.25 at 130 ℃ for different hydrothermal treatment time: (a) 24 h, (b) 36 h, (c) 60 h, and (d) 72 h.

above 130 ℃. The sheet-like products became distorted and further transformed into nanotubes upon an increase in the hydrothermal temperature.

The hydrothermal treatment time is known to be an important factor in nanotube growth. The effect of the hydrothermal treatment time was also investigated at the hydrothermal treatment temperature of 130 ℃. As shown in Figure 5, titanate phases were observed in all the samples and enhanced XRD peak intensities were observed for samples with longer hydrothermal treatment times. As shown in Figure 6, a remarkable change in morphology was observed after 24 h. The whisker-like titanate structures observed in TNT 24 h grew into TNTs, and the length increased. Additionally, we analyzed the nitrogen adsorption-desorption on the surface of the TNTs, and the results are listed in Table 1. When the hydrothermal time increased from 24 to 36 h, the specific surface area of the TNT drastically increased from 110.74 to 389.32 m^2 g^{-1}. However, a further increase in reaction time caused a slight decrease in the surface area and pore diameter, possibly due to partial transformation into titanate nanowires. Hwang et al. reported that TNTs can evolve into nanowires 50-300 nm in diameter and micrometers long by increasing the hydrothermal treatment time [21]. Zhu and Elsanousi reported that the transformation of nanotubes to nanowires occurred as a result of Ostwald ripening, in which smaller crystals dissolve

Table 1. Surface area, pore volume, and pore size of P25 and as-prepared TNT catalysts

Catalysts	Specific surface area (m^2/g)	Pore volume (cm^3/g)	Pore diameter (nm)
P25	50.72	0.15	12.56
TNT 24 h	132.96	0.33	8.37
TNT 36 h	389.32	1.34	12.44
TNT 60 h	377.36	1.23	11.55
TNT 72 h	318.44	1.53	9.58

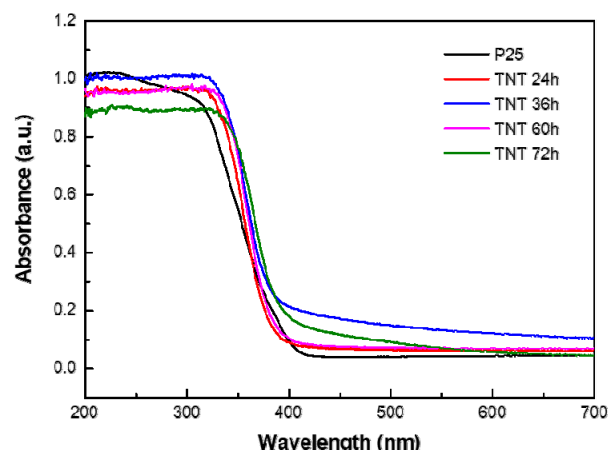**Figure 7.** FE-TEM images of TNT catalyst synthesized with TiO$_2$/NaOH ratio 0.25 at 130 ℃ for 36 h.

and redeposit on the larger crystals [22,23]. Therefore, the optimum hydrothermal treatment time was determined to be 36 h.

To identify the width and length of the TNTs, field-emission transmission electron microscopy (FE-TEM) images of TNT 36 h are displayed in Figure 7. The lengths and inner diameters of the synthesized TNTs were 30-145 nm and 2.6-4.9 nm, respectively. To compare our results to the available literature, a schematic diagram of the TNT formation is illustrated in Figure 8. According to previous studies and our results, a possible formation mechanism of titanate nanotubes can be explained by the following two stages: i) transformation of TiO$_2$ nanoparticles to nanosheets and ii) conversion of nanosheets to nanotubes by wrapping [14,21,24]. TiO$_2$ nanoparticles firstly dissolved in a concentrated alkaline solution by breaking the Ti-O-Ti bonds. The dissolved TiO$_2$ species generated [Ti(OH)$_6$]$_2$ during hydrothermal treatment and formed thin titanate nanosheets of layered Na$_2$Ti$_3$O$_7$, which possessed Na$^+$ ions between the individual layers of TiO$_6$. After acid treatment, Na$_2$Ti$_3$O$_7$ was converted to H$_2$Ti$_3$O$_7$ as the Na$^+$ ions were substituted with H$_3$O$^+$ ions. The Ti-O-Na bonds were then converted into Ti-OH bonds, which was ascribed to the continuous dehydration of the intermediate nanosheet-like layered structures, resulting in exfoliation owing to unequal surface tension on the nanosheets. Finally, the tops of the nanosheets were bent and rolled into large diameters and the TNTs were obtained.

Figure 9 shows the UV-Vis absorbance spectra of TiO$_2$ nanoparticles and TNTs. The band gap was calculated using the equation $Eg = 1240/\lambda_{abs}$, where λ_{abs} is the wavelength (nm). The absorption onset wavelength of P25 was 381 nm, which corresponded to a band gap of 3.25 eV, while the as-prepared TNT catalysts showed a slight red-shift, in accordance with the results


Figure 9. UV-vis spectra of P25 and as-prepared TNT catalysts.

of Li et al. [25], indicating a lower band gap than that of P25. This is ascribed to dimensional and size effects. According to Mowbray et al., lower-dimensional TiO$_2$ tends to have a higher band gap and lower photocatalytic activity owing to the quantum confinement effect [26]. Tao et al. reported a two-dimensional phase of TiO$_2$ with a remarkably reduced band-gap energy compared to that of common bulk phase TiO$_2$ [27]. In addition, semiconductor components are also dependent on their nanoscale size [28]. The volume-to-surface area ratio alters the number of surface atoms and orbital overlap, leading to an increase in the band-gap energy. To conclude, the reduced band-gap energy in TNT resulted from an increase in both particle size and dimension.

3.2. Photocatalytic activity

The prepared TNTs and P25 were evaluated through the photocatalytic degradation of MV under UV irradiation. The degradation efficiency was confirmed by measuring the absorbance intensity at 583 nm via UV-Vis spectroscopy. Figure 10(a) shows the experimental results obtained at an MV concentration of 30 ppm and catalyst amount of 1 g L^{-1}. P25 exhibited an absorption of 9.4% when stirred in the dark. In contrast, all TNT catalysts exhibited higher absorption abilities, indicating that more MV molecules were absorbed on the TNT surface, as the catalysts had larger specific surface areas ranging from 318.44 to 389.32 m^2 g^{-1}, while P25 only had a specific surface area of 50 m^2 g^{-1}. When

Figure 8. Schematic illustration for the synthesis procedure of TNT catalyst.
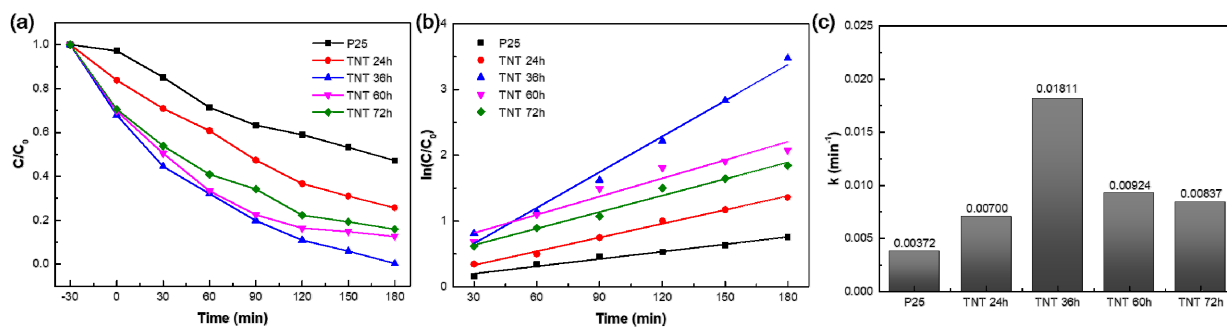
Figure 10. (a) Photocatalytic degradation of MV, (b) degradation rate of MV, and (c) kinetic rate over P25 and as-prepared TNT catalysts.

the UV lamp was turned on, the MV concentration over P25 gradually decreased and reached a degradation efficiency of 47.2% in 180 min. The four TNT catalysts clearly showed higher degradation efficiencies compared to P25. Among the TNT catalysts, TNT 36 h had the highest degradation efficiency (96.9%) under UV irradiation for 30 min. The order of degradation efficiency was consistent with that of the specific surface area results and was as follows: TNT 36 h > TNT 60 h > TNT 72 h > TNT 24 h.

To study the kinetic effect, the pseudo-first-order equation based on degradation was expressed as $\ln(C_0/C) = kt$, where C_0 is the initial concentration of MV, C is the final concentration of MV, t is the time (min), and k is the photodegradation rate constant (min^{-1}). The regression coefficients for the pseudo-first-order model for all catalysts were in the range of 0.9337-0.9932. The calculated kinetic rate constants are shown in Figure 10(b), where it is apparent that the MV degradation rate decreased in the following order: TNT 36 h (0.001811 min^{-1}) > TNT 60 h (0.00924 min^{-1}) > TNT 72 h (0.00837 min^{-1}) > P25 (0.00372 min^{-1}). These results suggest that the surface area and band-gap energy influence the degradation rate under UV irradiation. More specifically, TNT 36 h, which had the largest specific surface area among the catalysts, resulted in the highest degradation rate, whereas the lowest specific surface area of the P25 catalysts led to the lowest degradation rate. Moreover, the activity of TNT 36 h was 4.8 times higher than that of P25. It was assumed that the large surface area facilitated the adsorption and diffusion of MV molecules on the photocatalyst surface. Amano et al. revealed that photocatalytic activity is proportional to the specific surface area because the electron-hole recombination rate is much faster than the surface reaction rate [29]. In addition, larger surface areas can provide more active sites for photocatalytic degradation. Thus, we can conclude that specific surface area played a dominant role in the photodegradation of dye molecules.

4. Conclusions

In this study, TNTs were synthesized via an alkaline hydrothermal treatment using commercial TiO$_2$ P25. The TNTs were generated at a TiO$_2$/NaOH ratio of 0.25 by sufficiently dissolving TiO$_2$, breaking

the original Ti-O-Ti bonds, and generating new Ti-O-Ti bonds as titanate nanosheets, which are precursors of nanotubes. The hydrothermal treatment temperature and time were the driving forces for the formation and growth of the TNTs. High temperature and sufficient time allowed the TiO$_2$ nanoparticles to convert to TNTs; however, a hydrothermal time longer than 36 h led to a decrease in the specific surface area, which is attributed to the partial morphological transformation from nanotubes to nanowires. TNT with the largest surface area (389.32 m^2 g^{-1}) was obtained under the following conditions: TiO$_2$/NaOH ratio of 0.25, hydrothermal temperature of 130 ℃, and hydrothermal time of 36 h. To observe the photocatalytic activity of the TNTs, the photocatalytic degradation of MV over the catalysts was evaluated. A photodegradation efficiency of 96.9% was attained over TNT 36 h under UV irradiation for 180 min. In addition, TNT 36 h was 4.8 times more efficient than P25 because its large surface area allowed more contact between the MV molecules and OH radicals to degrade them efficiently. These results suggest that large surface area is an important factor in photocatalytic activity.

Acknowledgement

References

1. Jitan, S.A., Palmisano, G., and C. Garlisi, "Synthesis and surface modification of TiO$_2$-based photocatalysts for the conversion of CO$_2$," *Catalysts*, **10**(2), 227 (2020).
2. Yang, Y., Li, J., "TiO$_2$: A Critical interfacial material for incorporating photosynthetic protein complexes and plasmonic nanoparticles into biophotovoltaics," in Application of Titanium Dioxide, London, United Kingdom, IntechOpen (2017).
3. Kim, Y. E., Byun, M. Y., Lee, K.-Y., and Lee, M. S., "Effects of chlorinated Pd precursors and preparation methods on properties and activity of Pd/TiO$_2$ catalysts," *RSC Adv.*, **10**(68), 41462-41470 (2020).

4. Qu, J. and Lai, C., "One-dimensional TiO_2 nanostructures as photoanodes for dye-sensitized solar cells," *J. Nanomater.*, **2013**, 762730 (2013).

5. Feng, T., Feng, G. S., Yan, L., and Pan, J. H., "One-dimensional nanostructured TiO_2 for photocatalytic degradation of organic pollutants in wastewater," *Int. J. Photoenergy*, **2014**(1), 563879 (2014).

6. Li, Y., Guo, M., Zhang, M., and Wang, X., "Hydrothermal synthesis and characterization of TiO_2 nanorod arrays on glass substrates," *Mater. Res. Bull.*, **44**(6), 1232-1237 (2009).

7. Yu, Y., Zhang, P. Guo, L., Chen, Z., Wu, Q., Ding, Y., Zheng, W., and Cao, Y., "The design of TiO_2 nanostructures (nanoparticle, nanotube, and nanosheet) and their photocatalytic activity," *J. Phys. Chem. C*, **118**(24), 12727-12733 (2014).

8. Kasuga, T., Hiramatsu, M., Hoson, A., Sekino, T., and Niihara, K., "Formation of titanium oxide nanotube," *Langmuir,* **14**(12), 3160-3163 (1998).

9. Tsvetkov, N., Larina, L., Kang, J. K., and Shevaleevskiy, O., "Sol-gel processed TiO_2 nanotube photoelectrodes for dye-sensitized solar cells with enhanced photovoltaic performance," *Nanomaterials*, **10**(2), 296 (2020).

10. Cossuet, T., Rapenne, L., Renou, G., Appert, E., and Consonni, V., "Template-assisted growth of open-ended TiO_2 nanotubes with hexagonal shape using atomic layer deposition," *Cryst. Growth Des.*, **21**(1), 125-132 (2021).

11. Kim, M., Shin, N., Lee, J., Lee, K., Kim, Y.T., and Choi, J., "Photoelectrochemical water oxidation in anodic TiO_2 nanotubes array: Importance of mass transfer," *Electrochem. Commun.*, **132**, 107133 (2021).

12. López Zavala, M. Á., Lozano Morales, S. A., and Ávila-Santos, M. "Synthesis of stable TiO_2 nanotubes: Effect of hydrothermal treatment, acid washing and annealing temperature," *Heliyon*, **3**(11), e00456 (2017).

13. Kasuga, T., Hiramatsu, M., Hoson, A., Sekino, T., and Niihara, K., "Titania nanotubes prepared by chemical processing," *Adv. Mater.*, **11**(15), 1307-1311 (1999).

14. Yang, J., Du, J., Li, X., Liu, Y., Jiang, C., Qi, W., Zhang, K., Gong, C., Li, R., Luo, M., and Peng, H., "Highly hydrophilic TiO_2 nanotubes network by alkaline hydrothermal method for photocatalysis degradation of methyl orange," *Nanomaterials*, **9**(4), 526 (2019).

15. Li, P., Wang, J., Liu, L., Ma, J., Ni, Y., Wang, H., and Song, Y., "The effect of atmospheric pressure on the growth rate of TiO_2 nanotubes: Evidence against the field-assisted dissolution theory," *Electrochem. Commun.*, **132**, 107146 (2021).

16. Baszczuk, A., Jasiorski, M., and Winnicki, M., "Low-temperature transformation of amorphous sol–gel TiO_2 powder to anatase during cold spray deposition," *J. Therm. Spray Technol.*, **27**(8), 1551-1562 (2018).

17. Muniyappan, S., Solaiyammal, T., Sudhakar, K., Karthigeyan, A., and Murugakoothan, P., "Conventional hydrothermal synthesis of titanate nanotubes: Systematic discussions on structural, optical, thermal and morphological properties," *Mod. Electron. Mater.*, **3**(4), 174-178 (2017).

18. Huang, J., Cao, Y., Huang, Q., He, H., Liu, Y., Guo, W., and Hong, M., "High-temperature formation of titanate nanotubes and the transformation mechanism of nanotubes into nanowires," *Cryst. Growth Des.*, **9**(8), 3632-3637 (2009).

19. Li, J., Wang, Z., Zhao, A., Wang, J., Song, Y., and Sham, T. K., "Nanoscale clarification of the electronic structure and optical properties of TiO_2 nanowire with an impurity phase upon sodium intercalation," *J. Phys. Chem. C*, **119**(31), 17848-17856 (2015).

20. Joo, J. B., Zhang, Q., Lee, I., Dahl, M., Zaera, F., and Yin, Y., "Mesoporous anatase titania hollow nanostructures though silica-protected calcination," *Adv. Funct. Mater.*, **22**(1), 166-174 (2012).

21. Huang, J., Cao, Y., Huang, Q., He, H., Liu, Y., Guo, W., and Hong, M., "High-temperature formation of titanate nanotubes and the transformation mechanism of nanotubes into nanowires," *Cryst. Growth Des.*, **9**(8), 3632-3637 (2009).

22. Li, F., Liang, J., Zhu, W., Song, H., Wang, K., and Li, C., "Hydrogenation of *m*-chloronitrobenzene over different morphologies Ni/TiO_2 without addition of molecular hydrogen," *Catalysts*, **8**(5), 2-13 (2018).

23. Kim, S. G., Dhandole, L. K., Lim, J. M., Chae, W. S., Chung, H. S., Oh, B. H., and Jang, J. S., "Facile synthesis of ternary TiO_2 NP/Rh & Sb-codoped TiO_2 NR/titanate NT composites photocatalyst: Simultaneous removals of Cd^{2+} ions and Orange (II) dye under visible light irradiation ($\Lambda \geq 420$ nm)," *Appl. Catal. B Environ.*, **224**, 791-803 (2018).

24. Leng, M., Chen, Y., and Xue, J., "Synthesis of TiO_2 nanosheets via an exfoliation route assisted by a surfactant," *Nanoscale*, **6**(15), 8531-8534 (2014).

25. Li, C., Zong, L., Li, Q., Zhang, J., Yang, J., and Jin, Z., "Photocatalytic oxidation of propylene on Pd-loaded anatase TiO_2 nanotubes under visible light irradiation," *Nanoscale Res. Lett.*, **11**(1), 271 (2016).

26. Mowbray, D.J., Martinez, J. I., Lastra, G. J. M., Thygesen, K. S., and Jacobsen, K. W., "Stability and electronic properties of TiO_2 nanostructures with and without B and N doping," *J. Phys. Chem. C.*, **113**(28), 12301-12308 (2009).

27. Tao, J., Luttrell, T., and Batzill, M., "A two-dimensional phase of TiO_2 with a reduced bandgap," *Nat. Chem.*, **3**(4), 296-300 (2011).

28. Singh, M., Goyal, M., and Devlal, K., "Size and shape effects on the band gap of semiconductor compound nanomaterials," *J. Taibah Univ. Sci.*, **12**(4), 470-475 (2018).

29. Amano, F., Nogami, K., and Ohtani, B., "Visible light-responsive bismuth tungstate photocatalysts: Effects of hierarchical architecture on photocatalytic activity," *J. Phys. Chem. C.*, **113**(4), 1536-1542 (2009).